Petroleum Science 21 (2024) 1992–2004

Contents lists available at ScienceDirect

Petroleum Science

journal homepage: www.keaipublishing.com/en/journals/petroleum-science

Original Paper

Analysis of mechanical strengths of extreme line casing joint considering geometric, material, and contact nonlinearities

Ji-Yun Zhang [a], Chi Peng [a, *], Jian-Hong Fu [a], Quan Cao [b], Yu Su [b], Jian-Yun Pang [a], Zi-Qiang Yu [a]

[a] Petroleum Engineering School, Southwest Petroleum University, Chengdu, 610500, Sichuan, China
[b] Engineering Technology Research Institute of CNPC Southwest Oil and Gas Field Company, Chengdu, 610017, Sichuan, China

ARTICLE INFO

Article history:
Received 8 June 2023
Received in revised form
26 February 2024
Accepted 26 February 2024
Available online 27 February 2024

Edited by Jia-Jia Fei

Keywords:
Extreme line casing
Elastic-plastic mechanics
Finite element analysis
Tensile strength
Collapse strength

ABSTRACT

To address the challenges associated with difficult casing running, limited annular space, and poor cementing quality in the completion of ultra-deep wells, the extreme line casing offers an effective solution over conventional casings. However, due to its smaller size, the joint strength of extreme line casing is reduced, which may cause failure when running in the hole. To address this issue, this study focuses on the CST-ZT Φ139.7 mm $\times$ 7.72 mm extreme line casing and employs the elastic-plastic mechanics to establish a comprehensive analysis of the casing joint, taking into account the influence of geometric and material nonlinearities. A finite element model is developed to analyze the forces and deformations of the extreme line casing joint under axial tension and external collapse load. The model investigates the stress distribution of each thread tooth subjected to various tensile forces and external pressures. Additionally, the tensile strength and crushing strength of the extreme line casing joint are determined through both analytical and experimental approaches. The findings reveal that, under axial tensile load, the bearing surface of each thread tooth experiences uneven stress, with relatively high equivalent stress at the root of each thread tooth. The end thread teeth are valuable spots for failure. It is observed that the critical fracture axial load of thread decreases linearly with the increase of thread tooth sequence. Under external pressure, the circumferential stress is highest at the small end of the external thread, leading to yield deformation. The tensile strength of the joint obtained from the finite element model exhibits a relative error of less than 7% compared to the analytical and experimental values, proving the reliability of the finite element model. The tensile strength of the joint is 3091.9 kN. Moreover, in terms of anti-collapse capability, the joints demonstrate higher resistance to collapse compared to the casing body, which is consistent with the test results where the pipe body experiences collapse and failure while the joints remain intact during the experiment. The failure load of the casing body under external collapse pressure is 87.4 MPa. The present study provides a basic understanding of the mechanical strengths of extreme line casing joint.

1. Introduction

With the continuous exploration of oil and gas worldwide, there has been a significant increase in the number of ultra-deep wells. The development of oil and gas reservoirs is now characterized by more demanding geological conditions, including longer well depth, and concomitant higher temperature and pressure (Ahmed and Nathan Meehan, 2016; Zhang and Chen, 2019; Wang et al., 2021; Zhang, 2020; Cao and Fang, 2021; Liu L.P. et al., 2022). The commonly used API standard thread joints cannot meet the requirements of complex well structures in ultra-deep wells. In such cases, the extreme line casing proves to be advantageous due to its unique features, such as non-coupling design, compact joint size, and a reduced risk of blockage inside the wellbore (Shi et al., 1998; Wang et al., 2014). Furthermore, the increased gap between the joints of the extreme line casing and the wellbore results in an improvement in cementing quality, especially in small wellbores (Guo and Zhao, 2019). Despite of its advantages, it should be noted that the use of extreme line casing joints, which involve a decrease in the outer diameter of the joint, leads to a certain deterioration in

* Corresponding author.
E-mail address: pengchiswpu@swpu.edu.cn (C. Peng).

https://doi.org/10.1016/j.petsci.2024.02.014

the joint strength compared to conventional API casing joints. Specifically, the tensile strength of the joint in extreme line casing is lower than that of the conventional API casing joint (Gao et al., 2007). Therefore, conducting comprehensive research on the strength and integrity of extreme line casing joints holds great significance, which helps to minimize the occurrence of failures in the extreme line casing joint and optimize the thread structure of the extreme line casing joints.

Starting from the 1990s, the rise of deep and ultra-deep wells has posed significant challenges to the integrity of oil and gas wells. As a result, scholars initiated research on the design and manufacturing of tubing and casing joints. These researches aimed to address the specific requirements and complexities associated with the smaller wellbore resulting from increased well depth (Hilbert and Kalil, 1992; Klementich et al., 1995). In recent years, there has been significant progress in both theoretical and experimental research on the mechanical characteristics of casing joints. Meza et al. (2016) developed the VAM21 thread joint, which enables casing to withstand extremely harsh high-temperature and high-pressure conditions. The tensile, compressive, internal, and collapse strength of the VAM21 thread joint can reach 100% of the casing body. Huang et al. (2016) introduced a direct-connected special thread joint specifically designed for Φ139.7 mm $\times$ 7.72 mm 140 steel casing developed for window milling operations. Hu (2017) conducted finite element calculations and determined that the HSM-2 special thread joint demonstrated the ability to maintain a significant contact pressure and seal length, resulting in a high sealing index. The development and application of the small BG-FJU extreme line joint enabled “cementing inside casing" and multiple fracturing operations (Sun et al., 2022), which allowed for the successful re-stimulation and enhanced recovery of old wells.

The tensile strength and collapsing strength are crucial parameters that characterize the extreme line casing joint. Researchers have conducted certain studies on these aspects. These investigations aimed to better understand the performance and reliability of special thread joints under various loading conditions. By analyzing and improving the tensile and collapsing strengths, researchers have contributed to enhancing the overall integrity of casing (Li et al., 2014; Silva et al., 2019; Pan, 2019).

In high-temperature environments, the tensile resistance of thread joints will decrease as the temperature rises. This reduction in tensile strength has detrimental effects on the integrity of joints. The primary factors influencing the resistance of special thread joints are the material's yield strength, joint outer diameter, and wall thickness. By improving the yield strength and wall thickness, the casing can exhibit exceptional resistance to external collapse. It is worth noting that under non-uniform external loads, the special thread joint experiences the elastic stage, hardening stage, and stable stage.

To theoretically investigate the mechanical strength of casing joints, scholars have extensively utilized the finite element method to conduct numerical simulations. Bai et al. (2013) performed finite element analysis on the sealing performance of special thread joints. The analysis considered various conditions, including tightening, stretching, internal pressure, and temperature. In a subsequent study (Bai et al., 2015), the researchers investigated the influence of different bearing surface angles on the strength of special thread joints. Using the finite element method, they examined the effects of tensile load on joints and analyzed the behavior and performance of joints under different scenarios. Cui et al. (2015) conducted a study on the effects of make-up torque on two different types of special casing joints. They developed two-dimensional finite element models for these joints. Through parameter analysis, the researchers determined the failure conditions. Cirimello et al. (2016) took into account the actual operational processes in real drilling conditions and the influence of joint geometry and investigated the special thread joints. The study aimed to improve the understanding and application of special thread joints in on-site drilling operations. Li et al. (2018) utilized the finite element analysis to study the thread-sealing performance of special casing joints under typical working conditions. Their research provided valuable insights into the sealing capacity of special thread joints in practical applications. Focusing on the effects of the ellipse degree, Zhang et al. (2019) introduced the theory of sealing contact energy and analyzed the stress distribution in the conical surfaces of special thread joints. In 2019, Xu H. et al. (2019) introduced an integrity evaluation method specifically designed for special thread joints of casing. Their research focused on assessing the overall integrity and reliability of casing joints. Xu Z.Q. et al. (2019) proposed a calculation method using elastic mechanics to determine the joint strength of the API thread joint, which considered the replenished torque generated by the shoulder and aimed to prevent shoulder separation under the limited axial working load. Guo (2022) proposed an extreme line casing joint structure through finite element analysis and referencing the API 5C5 standard. This joint structure demonstrated satisfying anti-adhesive performance, high connection strength, and internal strength.

In synthesizing the findings of prior research, substantial progress has been made in understanding the sealing performance and behavior of extreme line casing joints under varied loading and environmental conditions. While the sealing performance and contact stress have been extensively explored, there is a notable gap in research concerning the connection strength and characteristics of thread teeth. The existing theoretical research exhibits disparities with the actual stress conditions experienced by extreme line casing joints.

This study aims to significantly contribute to the field by conducting a detailed analysis of the mechanical strength of the CST-ZT Φ139.7 mm $\times$ 7.72 mm extreme line casing joint, utilizing elastic-plastic mechanics. Differentiating itself from previous work, present approach carefully considers the geometric nonlinearity, material nonlinearity, and contact nonlinearity inherent in extreme line casing joint. The establishment of a comprehensive finite element model facilitates a numerical simulation that scrutinizes the contact stress of the thread tooth under axial tension and external collapse loads. Ultimately, the simulation results are meticulously compared with analytical and experimental data, substantiating the novelty and reliability of the finite element model. By focusing on these aspects, improvements can be made to enhance the overall performance and reliability of the extreme line casing joints. This work can serve as a valuable guide to ensuring the safety and reliability of extreme line casing in completion applications.

2. Finite element model of the extreme line casing joint

2.1. Nonlinearity of extreme line casing joint

2.1.1. Geometric nonlinearity

Under complex loads such as makeup torque, axial force, and internal and external extrusion pressure, the internal and external threads of the directly connected casing joint will experience significant relative displacement. At this point, the small deformation assumption is no longer applicable, so geometric nonlinearity needs to be introduced.

In a fixed Cartesian coordinate, the point position before deformation is denoted as X_i, while the point position after deformation is denoted as x_i. Then the displacement of the point can be

expressed as (Wang and Shao, 1997):

$$u_i = x_i(X_j) - X_i \tag{1}$$

In the initial state, the geometric shape of an element is obtained by interpolating the positions of the element nodes:

$$X' = \sum_{k=1}^{m} N_k X_k \tag{2}$$

The geometric shape can also be expressed by the same interpolation function and node displacement function. Using isoparametric elements, it is expressed as:

$$u' = \sum_{k=1}^{m} N_k u_k \tag{3}$$

The above two formulas can be simplified to:

$$X = NX^e,\ u = Nu^e \tag{4}$$

Combining all elements of the equilibrium equation, for a single element:

$$\boldsymbol{F} = \int V_0 \boldsymbol{N}^T \boldsymbol{p}_0 \mathrm{d}V + \int A_0 \boldsymbol{N}^T \boldsymbol{q}_0 \mathrm{d}V \tag{5}$$

According to the finite element theory, after the element balance equation is established, the nonlinear equation of the thread joint can be obtained through combination:

$$\boldsymbol{K}_S(u) \cdot u - \boldsymbol{F} = 0 \tag{6}$$

where X_i—the coordinate before the deformation of a point; x_i—coordinate of the point after deformation; u_i—displacement of the point; X_j—the new coordinate of the point after deformation; X_k—coordinate component of node k in the element; N_k—interpolation function associated with node k; m—number of nodes in a unit; X'—geometric shape of the unit; u_k—displacement component of node k in the element; u'—displacement of the element; N—interpolation function; X^e—sum of node deformations; u^e—sum of node displacements; $\boldsymbol{F}$—external force on the unit; V_0—volume before deformation; $\boldsymbol{N}^T$—transposition of linear strain displacement matrix; $\boldsymbol{p}_0$—volume force vector of the unit; A_0—area before deformation; $\boldsymbol{q}_0$—the surface force load vector of the element; $\boldsymbol{K}_S$—stiffness matrix of the element.

2.1.2. Material nonlinearity

In the stress distribution of casing joints, there is significant unevenness and pronounced stress concentrations in certain areas. As the external load reaches a certain threshold, these areas experience plastic deformation. At this point, the linear elastic stress-strain relationship is no longer applicable, and nonlinearity must be considered. It becomes necessary to incorporate the stress-strain relationship of the material, which exhibits nonlinear behavior.

In elastic-plastic incremental finite element analysis, the applied load is discretized into multiple small loads, each of which increases linearly. The linear analysis performed for each small load considers the linear relationship between stress and strain in the elastic state. As the load increases, the material may eventually enter the plastic deformation zone, where the stress-strain relationship becomes nonlinear.

Assume that the load and displacement u_i, strain ε_{ij}, and stress σ_{ij} at time t are known. When the time increases by Δt, according to the principle of virtual displacement, an incremental finite element equation for each linear incremental segment is established (Zhang, 2004):

$$\int_v \boldsymbol{B}^T \dot{\boldsymbol{\sigma}} \mathrm{d}V + \dot{\boldsymbol{F}} = 0 \tag{7}$$

$$\boldsymbol{K}_{ep}(\tau)\Delta\boldsymbol{u} = \Delta\boldsymbol{F} \tag{8}$$

$$\boldsymbol{K}_{ep}(\tau) = \sum_e \boldsymbol{K}^e_{ep}(\tau) \tag{9}$$

$$\boldsymbol{K}_{ep}(\tau) = \int_{v^e} \boldsymbol{B}^T \boldsymbol{D}_{ep}(\tau) \boldsymbol{B} \mathrm{d}V \tag{10}$$

$$\Delta\boldsymbol{F} = \boldsymbol{F}(t+\Delta t) - \boldsymbol{F}(t) = \sum_e \boldsymbol{F}^e(t+\Delta t) - \sum_e \boldsymbol{F}^e(t) \tag{11}$$

$$\boldsymbol{F}^e(t+\Delta t) = \int_{v_e} \boldsymbol{N}^T b(t+\Delta t)\mathrm{d}V + \int_{S_{e_r}} \boldsymbol{N}^T q(t+\Delta t)\mathrm{d}S \tag{12}$$

$$\boldsymbol{F}^e(t) = \int_{V_e} \boldsymbol{B}^T \boldsymbol{\sigma}(t)\mathrm{d}V \tag{13}$$

where $t \le \tau \le t + \Delta t$. If $\tau = t$, then it means using the starting tangent stiffness matrix method, where b represents the physical force, q represents the surface force, and the time in parentheses represents the corresponding moment of the mechanical quantity.

After solving $\Delta\boldsymbol{u}$ from Eq. (8), use the geometric relation $\Delta\boldsymbol{\varepsilon} = \boldsymbol{B}\Delta\boldsymbol{u}$ to get $\Delta\boldsymbol{\varepsilon}$, and then integrate according to the constitutive relation to decide $\Delta\boldsymbol{\sigma}$.

After obtaining the stress, substituting it into Eq. (7):

$$\Delta\overline{\boldsymbol{F}} = \boldsymbol{F}^e(t+\Delta t) - \boldsymbol{F}^e_i(t+\Delta t) = \sum_e \left[\int_{v_e} \boldsymbol{N}^T b(t+\Delta t)\mathrm{d}V + \int_{S_{e_r}} \boldsymbol{N}^T q(t+\Delta t)\mathrm{d}S \right] - \sum_e \int_{v_e} \boldsymbol{B}^T \boldsymbol{\sigma}(t+\Delta t)\mathrm{d}V \tag{14}$$

where $\boldsymbol{B}^T$—strain displacement matrix; $\dot{\boldsymbol{\sigma}}$—stress vector; $\dot{\boldsymbol{F}}$—node vector; $\boldsymbol{K}_{ep}(\tau)$—stiffness matrix; $\Delta\boldsymbol{u}$—displacement increment; $\Delta\boldsymbol{F}$—force increment; $\boldsymbol{D}_{ep}(\tau)$—material constitutive matrix; b—physical strength; q—surface force.

The unbalanced force vector, denoted as $\Delta\overline{\boldsymbol{F}}$, represents the residual forces that exist in the system at each iteration step of the solution. The balance equation is iteratively solved by updating the unknowns (such as displacement or strain) until the unbalanced force vector becomes small enough to indicate that the system has achieved balance. In each iteration, the unbalanced force is calculated based on the current state of the system and compared with the convergence criterion. The iterative process continues until the unbalanced force vector becomes small enough, indicating that a satisfactory solution has been achieved.

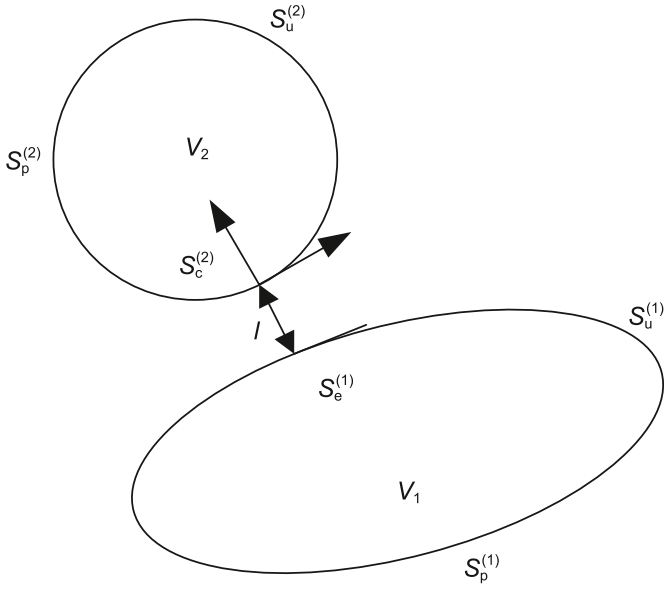

Fig. 1. Schematic diagram of two-body contact.

2.1.3. Contact nonlinearity

Fig. 1 depicts two objects in contact with each other. The contact areas are V_1 and V_2. The mechanical boundary equation describing the contact is $S^{(i)} = S_p^{(i)} + S_u^{(i)} + S_c^{(i)}$, where i represents two contact bodies ($i = 1, 2$), $S_p^{(m)}$ is the force boundary, $S_u^{(m)}$ is the displacement boundary, and $S_c^{(m)}$ is the possible contact boundary. In Fig. 1, l represents the gap space between the contact bodies at the beginning of each incremental step. A negative value of l means interference fit. During the contact simulation process of two objects, it is necessary to continuously evaluate and determine whether the two objects are in contact with each other.

The contact detection algorithm analyzes the geometric properties of objects to identify potential contact areas. It then examines factors like proximity distance and penetration depth to determine actual contact. If objects are too close or penetrate each other, contact is confirmed. This process is repeated at every simulation step to accurately depict interactions like friction and contact forces. $p_c = \{p_T, p_N\}^T$ is the force on the contact surface, and the local coordinate of the contact surface is represented by O-t-n. Then the three types of characteristics of the contact state can be expressed as follows (Zhang, 2004).

Separate state:

$$\mathrm{d}u_N^{(1)} - \mathrm{d}u_N^{(2)} + l > 0,\ p_N = p_T = 0 \tag{15}$$

Bonded state:

$$\begin{cases} \mathrm{d}u_N^{(1)} - \mathrm{d}u_N^{(2)} + l = 0,\ p_N = -\alpha_N\left(\mathrm{d}u_N^{(2)} - \mathrm{d}u_N^{(1)} - l^*\right) \\ \left|\mathrm{d}u_T^{(1)} - \mathrm{d}u_T^{(2)}\right| > 0,\ p_T = -\alpha_T\left(\mathrm{d}u_T^{(2)} - \mathrm{d}u_T^{(1)}\right) \end{cases} \tag{16}$$

Sliding state:

$$\begin{cases} \mathrm{d}u_N^{(1)} - \mathrm{d}u_N^{(2)} + l = 0,\ p_N = -\alpha_N\left(\mathrm{d}u_N^{(2)} - \mathrm{d}u_N^{(1)} - l^*\right) \\ \left|\mathrm{d}u_T^{(1)} - \mathrm{d}u_T^{(2)}\right| > 0,\ p_T = -\mu_f |p_N| sign\left(\mathrm{d}u_T^{(2)} - \mathrm{d}u_T^{(1)}\right) \end{cases} \tag{17}$$

where $\mathrm{d}u_N^{(m)}$ and $\mathrm{d}u_T^{(m)}$ are respectively the normal incremental displacement and tangential incremental displacement of the contact point; l^* represents the relative displacement of the contact body at the end of the incremental step; p_N and p_T represent the normal force and tangential force on the contact surface; μ_f is the coefficient of sliding friction; α_N and α_T are normal penalty parameter and tangential penalty parameter.

2.2. Material properties of the model

The casing thread contact problem involves an elastic-plastic large deformation analysis, which considers the behavior of the casing material under varying stress and strain conditions. The stress-strain curve of the CS-140V casing steel provides important information about the material's response to loading (Hengel, 2001). Fig. 2 illustrates the stress-strain curve, which shows the relationship between the applied stress and resulting strain for the CS-140V casing steel. This curve characterizes the material's elastic and plastic behavior, including its yield point, strain hardening, and ultimate strength.

Table 1 shows the mechanic parameters of the casing steel, including elastic modulus, yield strength, Poisson's ratio, and other relevant material properties. These parameters are crucial for conducting accurate finite element simulations and analyzing the casing thread contact problem.

It is necessary to use real stress and real strain when applying the plasticity data in numerical simulation. The obtained nominal stress and nominal strain in Fig. 2 are converted to real values through (Zhuang, 2009):

$$\varepsilon = \ln(1 + \varepsilon_{nom}) \tag{18}$$

$$\sigma = \sigma(1 + \varepsilon_{nom}) \tag{19}$$

According to Eqs. (18) and (19), the real stress-strain relationship can be obtained (Table 2).

2.3. Establishment of finite element model

The work focuses on the joint of CST-ZT Φ139.7 mm × 7.72 mm extreme line casing, as depicted in Fig. 3. The joint features a threaded section that is thickened by an additional 2 mm compared to the body of the casing. The bearing surface of the joint is inclined at an angle of −15°, while the guide surface has an angle of 45°.

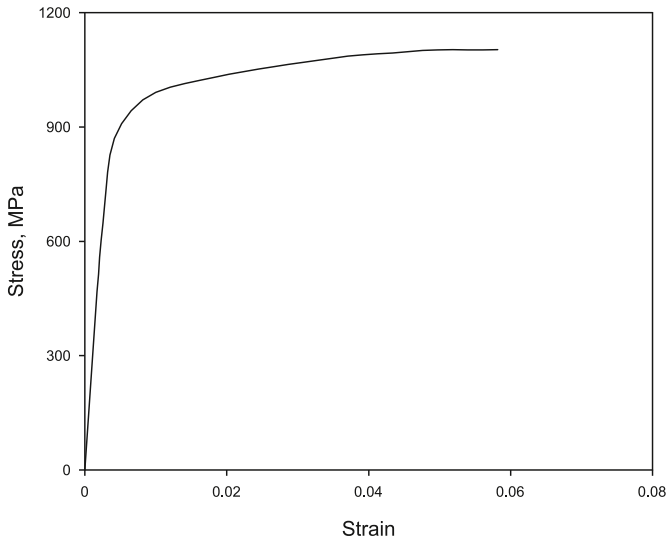

Fig. 2. Stress-strain curve of casing material.

Table 1
Mechanic parameters of CS-140V steel.

Steel grade	Elastic modulus, Pa	Poisson's ratio	Yield strength, MPa	Tensile strength, MPa
CS-140V	2.06×10^5	0.29	965	1034

Table 2
Real stress-strain relationship of CS-140V steel.

Nominal stress, MPa	Nominal strain	True stress, MPa	Real strain
0	0	0	0
427	0.0014	2.631444	0.000608
757	0.0027	2.879669	0.001171
925	0.0054	2.966611	0.002339
983	0.009	2.992995	0.003891
1009	0.0132	3.004321	0.005695
1030	0.018	3.013259	0.007748
1067	0.029474	3.028571	0.012615
1094	0.04483	3.039414	0.019046
1095	0.057957	3.039811	0.024468

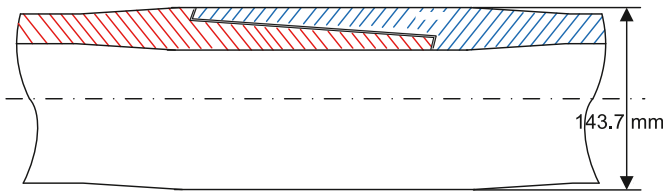

Fig. 3. Sectional view of extreme line casing joint.

These design characteristics play a crucial role in the performance of the joint. To provide further details, specific parameters of the internal and external threads of the casing joint are presented in Figs. 4 and 5. These figures outline the geometry and dimensions of the threads, including crest and root dimensions, flank angles, and other relevant specifications.

The rest of the basic parameters are shown in Table 3. The information provided in Figs. 3–5, and Table 2 serves as a foundation for the subsequent analysis and simulation conducted in the article.

2.3.1. Geometrical model and meshing

Considering the complexity of the casing joint structure and the computational challenges associated with establishing a three-dimensional finite element model, a two-dimensional axisymmetric model is employed in the simulation of thread forces. This modeling approach simplifies the analysis by reducing the problem from three-dimensional to two-dimensional, focusing on the radial symmetry of the casing thread.

By utilizing an axisymmetric model, the computational effort can be significantly reduced, as the number of elements and contact nodes is considerably smaller compared to a three-dimensional model. This enables efficient simulations and facilitates the analysis of the forces acting on the thread. While a two-dimensional

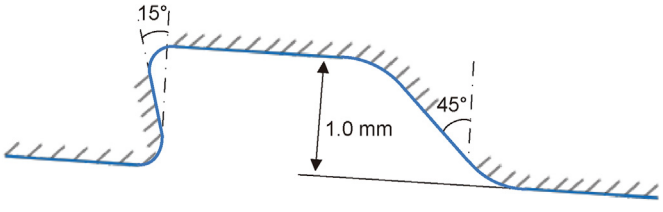

Fig. 4. Structure of the internal thread tooth of the casing joint.

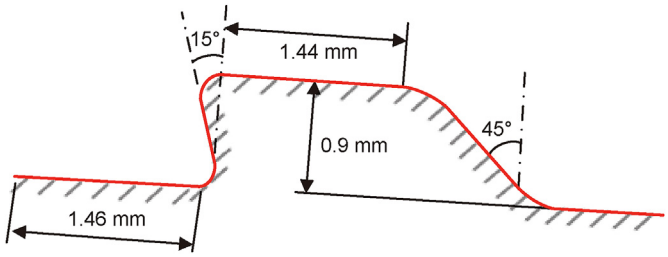

Fig. 5. Structure of the external thread tooth of the casing joint.

Table 3
Thread parameters of extreme line casing.

Symbol	Value	Unit	Symbol	Value	Unit	Symbol	Value	Unit
γ_t	3.58/2	°	r_{s0}	64.43	mm	r_0	71.85	mm
γ_s	5.71/2	°	L_s	3.94	mm	r_i	62.15	mm
E_7	69.75	mm	L	4.36	mm	μ	0.02	mm
L_7	41.32	mm	E	2.06e5	MPa	r_{shi}	62.32	mm
F_{rs}	1.46	mm	ν	0.29	/	r_{sho}	64.26	mm
φ	15	°	L_n	5.28	mm	T_A	1000	N·m

γ_t—half taper angle of thread; γ_s—half cone angle of sealing surface; φ—shoulder chamfer; E—elastic modulus; ν—Poisson's ratio; μ—friction coefficient; T_A—engagement torque; r_0—casing outer radius; r_i—casing inner radius; L—pitch; F_{rs}—the width at the bottom of the partial trapezoidal thread; r_{s0}—the radius at the nose end of the sealing surface; L_s—the axial length of the sealing surface; r_{shi}—the inner radius of the platform shoulder; r_{sho}—the outer radius of the platform shoulder; L_n—the axial length of the cone between the shoulder surface and the small end of the external thread; E_7—the diameter of the partial trapezoidal casing thread; L_7—the complete thread length of trapezoidal casing.

axisymmetric model may not capture all the intricacies of the three-dimensional behavior, it provides valuable insights into the mechanical response of the casing thread under various loading conditions. Indeed, the use of a two-dimensional model may result in some deviation from the real three-dimensional cases. However, the stress analysis of casing threads is radially symmetric, and the impact of the third dimension is limited (Cao, 2013; Cui, 2013; Xiang, 2016). Researchers have successfully utilized this modeling approach to investigate the performance and strength of casing threads (Zeng, 2004).

The geometrical model of the CST-ZT Φ139.7 mm × 7.72 mm extreme line casing joint is established, and a suitable mesh for finite element analysis is generated (Fig. 6). In this study, special attention is given to the thread surface, sealing surface, and shoulder, where local refinement of the mesh is applied to accurately capture the stress and strain distribution (Fig. 7). The mesh is carefully designed to ensure that it adequately represents the geometry of the casing and captures the critical areas of interest. The mesh used in the analysis consists of approximately 20,000 grids, providing a reasonable level of discretization for the problem at hand. To ensure the reliability and accuracy of the results, the independence of the mesh has been verified. This involves performing sensitivity analyses and convergence tests to assess the stability and convergence of the solution concerning changes in the mesh density. By employing a well-refined mesh and verifying its independence, the model is suitably prepared for subsequent

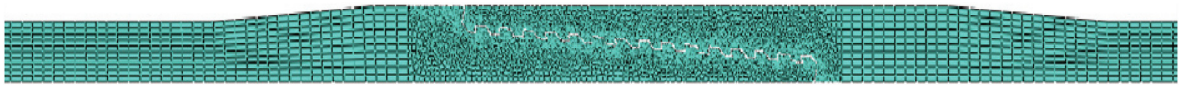

Fig. 6. Mesh of the casing joint model.

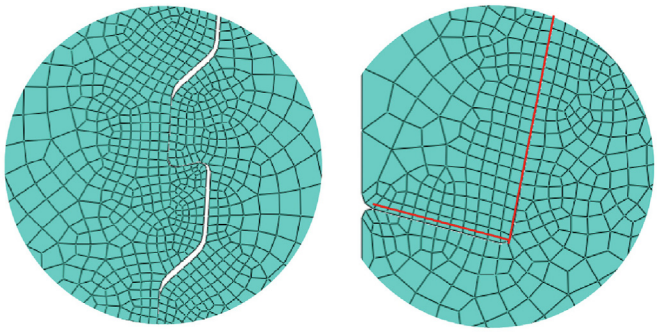

(a) Mesh refinement of thread segment.

(b) Mesh refinement of shoulder section and sealing surface.

Fig. 7. Mesh refinement.

analysis and evaluation of the mechanical behavior of the extreme line casing.

2.3.2. Boundary conditions

In the context of 2D axisymmetric models, directly applying torque to the model is not possible. Instead, alternative methods are employed to simulate the effect of torque. One commonly used approach, as described in previous studies (Chen, 2014; Xu, 2015), involves simulating the make-up process of the joint by introducing a certain amount of interference on the torque shoulder. To achieve this, the concept of interference contact is employed in the finite element analysis. Fig. 8 illustrates the application of this method. By defining the interference contact between the mating surfaces of the joint, the imposed interference effectively simulates the effect of torque during the make-up process. It allows for a realistic representation of the joint assembly process and facilitates the analysis of the mechanical characteristics and performance of the casing joint. The specific interference amount is decided by trial and error. It is found that the interference amount mainly affects the simulated tensile strength of the joint, while it does not lead to an obvious variation of the collapse strength. Different interference amounts have been used to find the best match between the simulated tensile strength of the joint and the test result. The optimal interference amount is found to be −0.24.

The boundary conditions for the tensile simulation and extrusion simulation of the extreme line casing are illustrated in Fig. 8(a) and (b). In Fig. 8(a), the movement on the right side of the casing is fully constrained, and the tensile load is uniformly applied to the left end of the section, which is set at 1200, 2000, and 3200 kN, respectively. In Fig. 8(b), the movement on both sides of the casing is fully constrained, and the extrusion load is uniformly applied to the top of the casing, which is set from 70 to 120 MPa.

2.3.3. Failure criterion of material

The Von Mises yield criterion is employed in the finite element numerical simulation to assess casing joint yield behavior. This criterion is widely used in numerical simulations to analyze the plastic deformation and failure of materials subjected to complex loading conditions. The criterion is based on the concept of equivalent stress and is defined as follows:

$$\sigma_i = \sqrt{\frac{1}{2}\left[(\sigma_1-\sigma_2)^2+(\sigma_2-\sigma_3)^2+(\sigma_1-\sigma_3)^2\right]} \tag{20}$$

where σ_i is the equivalent stress; σ_1, σ_2, and σ_3 are the principal stresses.

If the equivalent stress σ_i exceeds the yield strength σ_s of the CS-140V steel, it is considered as yielding or failure. The Von Mises yield criterion allows for a more comprehensive assessment of yielding compared to a uniaxial stress criterion. It considers the combined effect of all principal stresses on the material's yielding behavior, rather than focusing on a single principal stress.

3. Contact stress and strength of the extreme line casing joint

3.1. Equivalent contact stress of thread under axial tension

The simulated axial tensile forces applied to the Φ139.7 mm × 7.72 mm extreme line casing joint are 1200, 2000, and 3200 kN. The simulation results, as shown in Fig. 9, indicate that there is stress concentration at the root of each thread tooth. Among them, the stress concentration at the root of the first and last thread tooth is the most severe. Consequently, the failure of the thread tooth should initiate from the first or last thread root. The stress concentration at the thread root is a common phenomenon due to the abrupt change in geometry and the redistribution of stresses. The first and last thread teeth experience higher stress concentrations because they are closer to the ends of the threaded section, where the stress distribution is less uniform. It is important to note that stress concentration at the thread root can lead to localized plastic deformation and potential failure initiation. When the applied axial tension reaches 3200 kN, the loads on the first and the last thread tooth go beyond the critical value (965 MPa). As a result, the first and the last thread teeth are prone to failure. It is crucial to consider the strength and load-bearing capacity of the first thread tooth when designing and using the casing thread joint. Reinforcing the end thread teeth or modifying the joint design to distribute the load more evenly among the thread teeth can help prevent premature failure and enhance the overall performance and reliability of the joint.

Figs. 10–12 depict the variations of Von Mises stress, axial load, and contact pressure on each thread tooth. These figures demonstrate that when subjected to axial tension, the Von Mises stress, axial load, and contact pressure on the thread teeth all exhibit a saddle shape, with higher values on the sides and lower values in the middle. The saddle-shaped distribution of stress and load along the thread surface is a characteristic feature of thread joints. Specifically, it is observed that the first and last thread teeth bear the majority of the axial load. Due to the non-uniform distribution of forces and the thread geometry, the thread teeth located at the ends experience higher stresses and carry a larger portion of the axial load. This is why the first and last thread teeth are subjected to significant stress concentrations and are more susceptible to failure. When the tension load is 3200 kN, the average Mises stress at the first thread tooth reaches beyond 900 MPa, and the maximum local value is larger than the yield strength of the material.

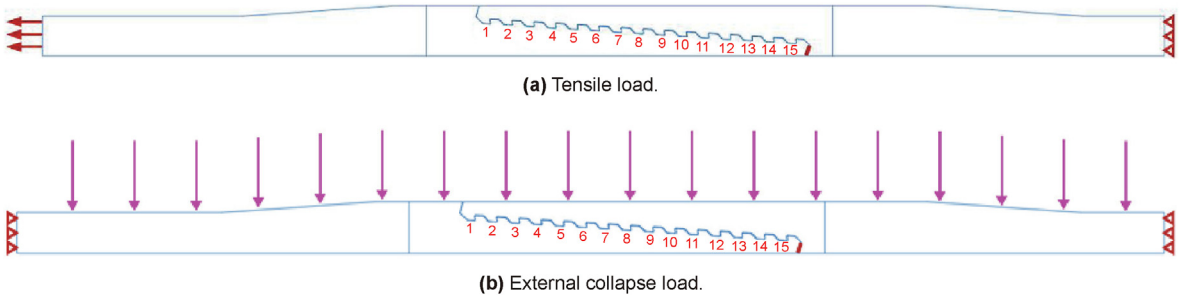

Fig. 8. Schematic diagram of joint load and boundary condition.

3.2. Simulation of thread equivalent contact stress of extreme line casing under external collapse load

The stress distributions of the extreme line casing joint under external pressures ranging from 70 MPa to 120 MPa are simulated. Typical results are shown in Fig. 13.

The maximum stress is found at the inner wall of the casing body, which is consistent with previous research (Sun et al., 2016; Lu, 2017; Lou et al., 2021; Lambrescu and Zisopol, 2023). Since the joint is thicker than the casing body, the stress at the inner wall of the joint is smaller than that of the casing body. As the external pressure increases, the Mises stress in the casing body and joint also increases. Once the external collapse load reaches 100 MPa, the maximum yield strength of steel is reached, and the casing body

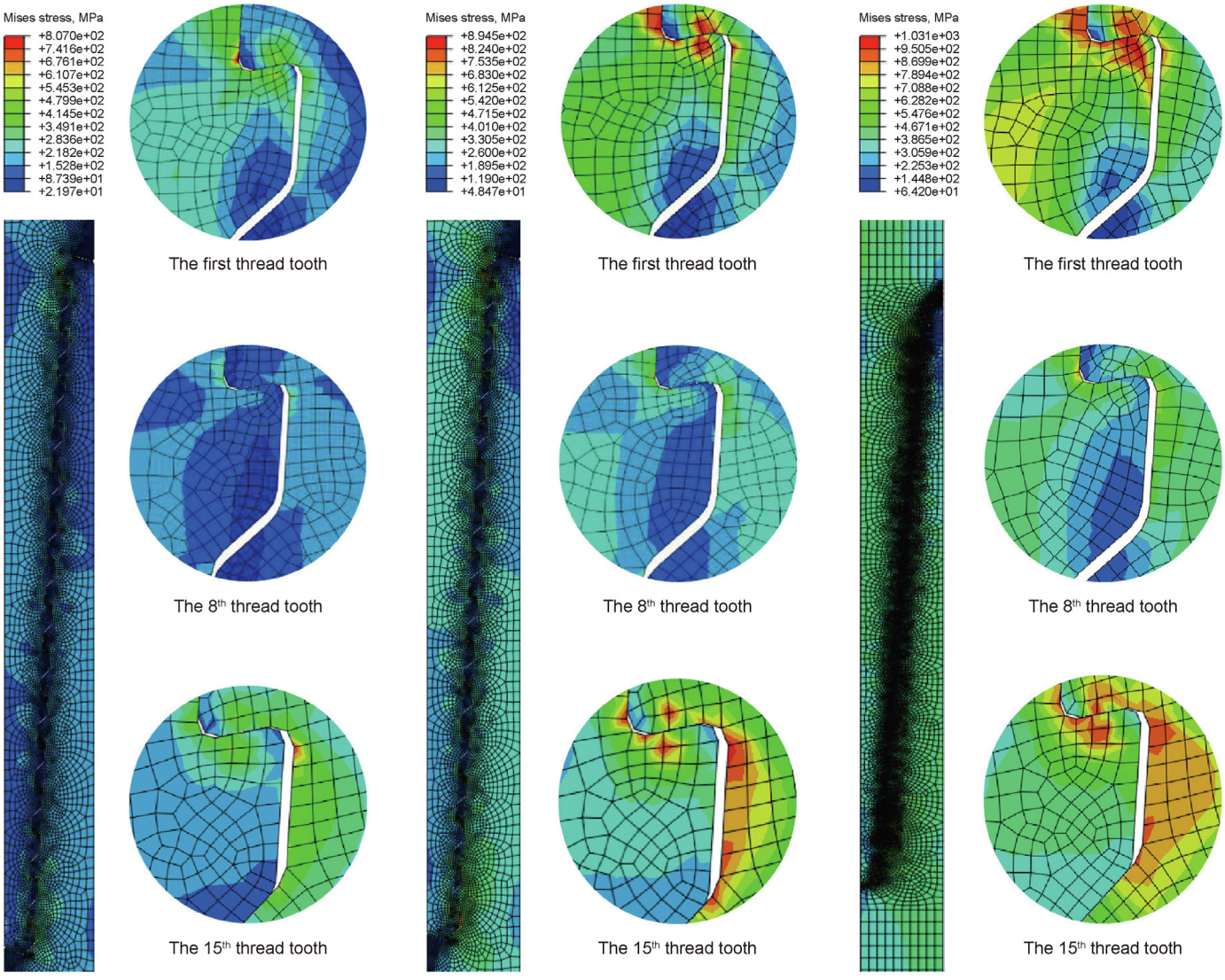

Fig. 9. Stress distribution of joint under axial tension of 1200, 2000, and 3200 kN.

begins to fail. Interestingly, the simulation reveals that the pipe body yields before the thread joint. Based on the simulation results, when the external pressure reaches 115 MPa, the casing joint starts to yield. Therefore, the predicted yield strength and collapse pressure of the thread joint are estimated to be approximately 115 MPa, which closely aligns with the value estimated from field operation.

4. Analytical solution of the strength of extreme line casing joint

4.1. Determination of tensile strength of extreme line casing joint

The critical axial load for tensile failure of CST-ZT Φ139.7 mm $\times$ 7.72 mm extreme line casing joints is less than that for shear failure, so the mechanical characteristics of joints under axial tension are analyzed. Under the axial tension on the casing, a fracture of the joint occurs when the thread of the joint undergoes tensile failure. The critical axial tension at the joint can be calculated by the following analytical formula (Shahani and Sharifi, 2009):

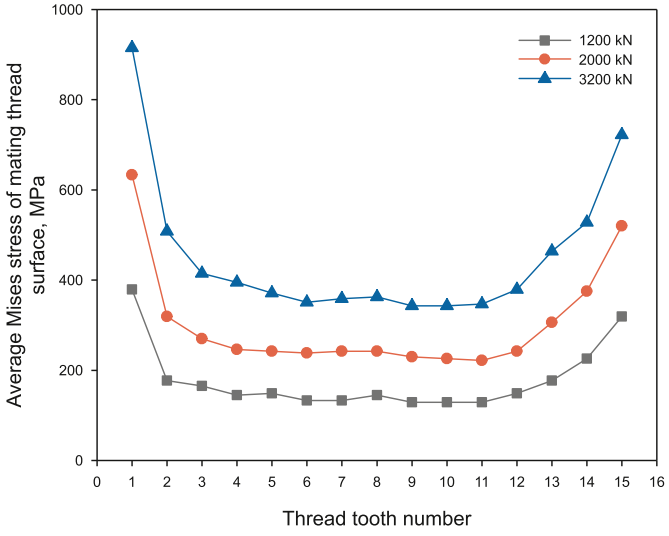

Fig. 10. Comparison of average Mises stress of mating thread surfaces under different tensions.

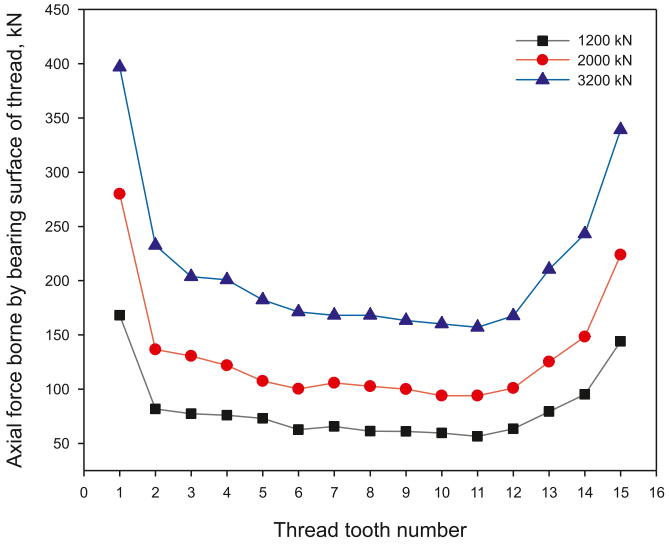

Fig. 11. Comparison of axial force distribution on thread-bearing surfaces under different tensile forces.

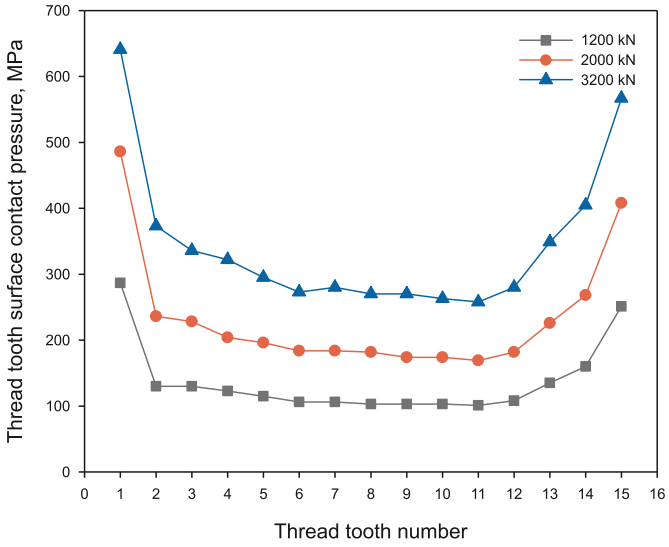

Fig. 12. Comparison of contact pressure on thread tooth surface under different tension.

$$F_{bt} = \frac{\pi}{4}\left[\left(\frac{d_p + D_{br}}{2}\right)^2 - D_i^2\right]\sigma_b \tag{21}$$

In the formula, F_{bt}—the axial tension when the threaded joint undergoes tensile fracture, kN; D_{br}—maximum diameter of external thread, mm; d_p—engaging diameter of the thread, mm; D_i—internal diameter of the casing, mm; σ_b—tensile strength of casing body, MPa.

Fig. 14 illustrates the comparison between the analytical value and the finite element simulation results for the critical axial load of the extreme line casing thread joint. The plot shows that the critical axial load for tensile failure linearly decreases with the increase in the sequence of thread. If the axial load on any thread exceeds the critical value at that particular cross-section, thread fracture will occur. When the axial tension is 3200 kN, the axial load at the first thread tooth reaches the critical value, so the fracture of the first thread tooth will happen. It's important to note that the specific values shown in Fig. 14 are specific to the CST-ZT Φ139.7 mm $\times$ 7.72 mm extreme line casing and the corresponding thread design. The relationship between the number of threads and the fracture critical axial load may vary for different casing sizes, thread geometries, and material properties.

4.2. Determination of collapse strength of extreme line casing joint

Fig. 15 illustrates the loads on casing joint threads, revealing the two primary forces acting upon the threads: the external collapse load P and the interference contact. According to the thick-walled cylinder theory, it can be concluded that the circumferential stress at the inner surface of the external thread reaches the yield strength of CS-140V steel first, resulting in the failure of the casing joint. Hence, the circumferential stress of the external thread is utilized for analyzing the joint strength subjected to external collapse pressure.

The equation for calculating the collapse strength of the extreme line casing joint is:

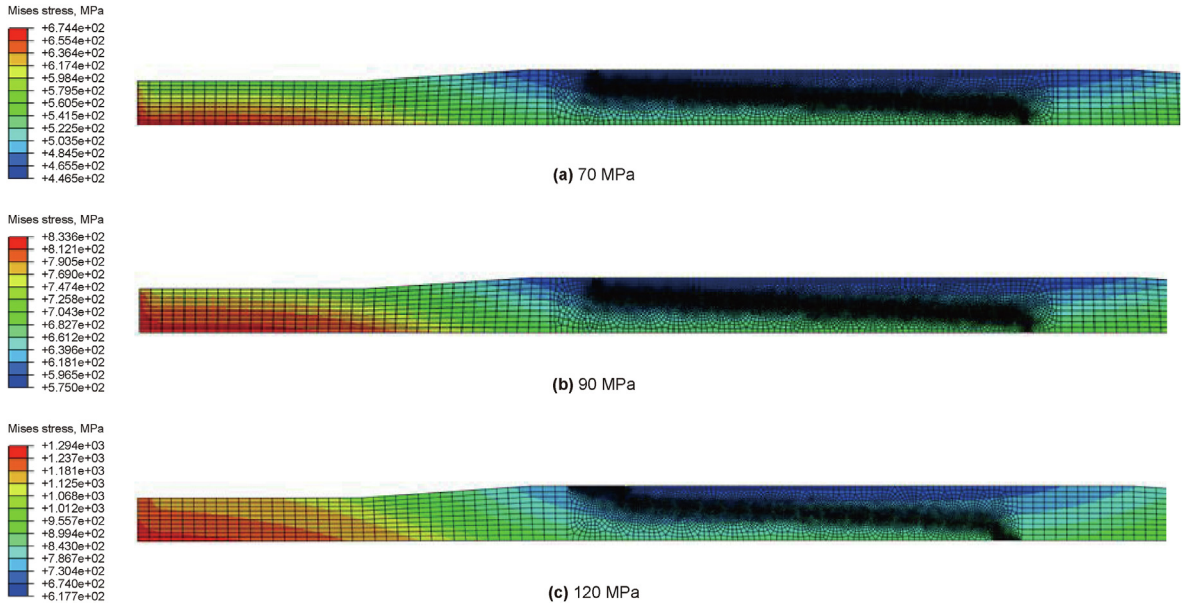

Fig. 13. Finite element simulation of casing collapse strength.

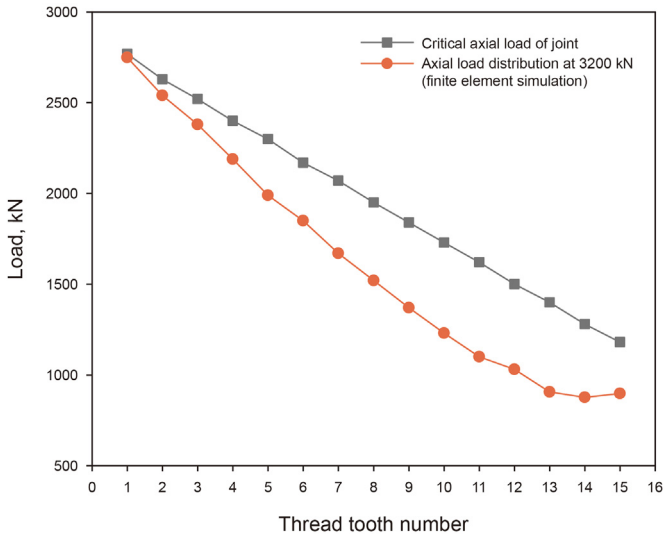

Fig. 14. Failure load curve of joint fracture.

$$\sigma_\theta = \sigma_{\theta 1} + \sigma_{\theta 2} \tag{22}$$

where σ_θ—the total circumferential stress generated on the inner surface of the internal thread, MPa; $\sigma_{\theta 1}$—the circumferential stress produced by the external collapse load on the inner surface, MPa; $\sigma_{\theta 2}$—the circumferential stress on the inner surface caused by thread interference, MPa.

$\sigma_{\theta 1}$ and $\sigma_{\theta 2}$ are calculated by:

$$\sigma_{\theta 1} = -\frac{2Pr_o^2}{r_o^2 - r_i^2} \tag{23}$$

$$\sigma_{\theta 2} = -\frac{2P_{cr}r_c^2}{r_c^2 - r_i^2} \tag{24}$$

P—the external collapse load on the joint, MPa; P_{cr}—contact surface pressure generated by thread surface interference δ, MPa; r_o—outer radius of joint, mm; r_i—inner radius of joint, mm; r_c—radius of contact surface, mm.

According to Table 3, $r_o = 71.85$ mm, $r_i = 62.13$ mm, interference $\delta = 0.04$ mm. CS-140V steel yield strength $Y_p = 965$ MPa, external collapse load $P = 115$ MPa. Starting from the large end of the external thread, the comparison of theoretically calculated circumferential stress by Eq. (22) and finite element simulation results is shown in Fig. 16. Fig. 16 demonstrates that there is a good level of agreement between the theoretical value and finite element solution at the small end of the thread. However, a significant error is observed at the large end of the joint. This discrepancy can be attributed to the fact that the theoretical model does not take into account the impact of the thickened transition section and the shoulder. These structural elements can affect the stress distribution and lead to deviations between the theoretical and simulation results. Additionally, it is evident that the circumferential stress at the small end of the external thread is the highest, and it experiences yielding first. This finding highlights the critical location where failure is likely to initiate due to the maximum stress concentration. Understanding this stress distribution is vital for identifying potential failure modes and designing appropriate measures to enhance the strength and durability of the joint.

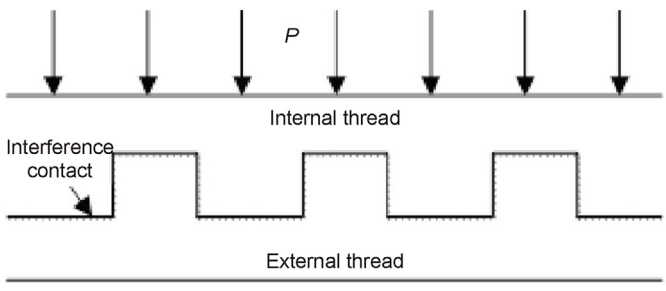

Fig. 15. Loads of casing joint threads.

5. Strength test of CST-ZT Φ139.7 mm × 7.72 mm extreme line casing

5.1. Tensile strength test

The strength test of CST-ZT Φ139.7 mm × 7.72 mm extreme line casing follows the API standard RP 5C5-2017. Test results are listed in Table 4, and the typical casing morphology after the failure test is shown in Fig. 17. A total of 5 tests are conducted. The tensile failure mode of the CST-ZT extreme line casing involves the fracture of the pipe body and the fracture at the root of the external thread, which is in line with the numerical prediction of the vulnerable position of the joint. Specifically, the casing body fractures only once, while the external thread experiences fracture four times. The tensile load for casing body failure (3900.9 kN) is much higher than that for joint failure. The average failure load of the thread is 3092.4 kN. This value represents the average axial tension at which the thread fractures and fails.

5.2. Collapse strength test

Test results of collapse strength are shown in Table 5, and the morphology of the casing after collapse failure is shown in Fig. 18. Based on the collapse strength test results, it is determined that the failure in all 5 samples occurred in the casing body, while the casing joint remains intact. This implies that the collapse strength of the extreme line casing joint is greater than that of the casing body. Furthermore, the average collapse strength of the casing body is 87.4 MPa. This value represents the load at which the casing body undergoes collapse failure.

The tensile strength and collapse strength are important parameters for evaluating the strength and performance of the joint under axial tension. By determining the average failure loads, engineers can establish design criteria and guidelines to ensure the safe and reliable operation of the CST-ZT extreme line casing in practical applications.

5.3. Comparison of finite element simulation results with analytical and experimental strengths

Table 6 and Table 7 present a comparison between the finite element results, analytical solutions, and test values. The average value of the joint's tensile strength, as determined by the tests, is 3092.4 kN. From Tables 6 and it can be observed that the relative error between the analytical solution, the finite element solution, and the test value is less than 7%. This indicates that the tensile strength of the joint calculated by the finite element model established in this study is accurate. Additionally, Table 7 reveals that the collapse strength of the joints is greater than that of the casing body. This finding aligns with the test results, where the casing body experiences collapse failure while the joints remain intact during the anti-collapse test. The collapse strength of the casing body is determined to be 87.4 MPa. These comparisons and observations further validate the reliability and accuracy of the finite element model in predicting the mechanical behavior and failure characteristics of the extreme line casing joint.

In addition, the relative errors of tensile strength between the finite element results and experimental results under different combinations of nonlinearities are achieved by keeping certain nonlinearity settings in the numerical model, as shown in Fig. 19. From the figure, it can be observed that considering the effects of three nonlinearity results in the smallest relative error between the simulation and experimental results, providing the best match of the actual tensile strength of the casing joint. The less nonlinearities considered, the larger the relative error. Additionally, the results indicate that the three nonlinearities have varying degrees of influence, with contact nonlinearity having the greatest impact on the simulation results, followed by geometric nonlinearity, and material nonlinearity having the smallest effect. Therefore, by accounting for these three nonlinearities, present model

Table 4
Results of tensile strength test.

Sample No.	Failure tensile load, kN	Failure location and failure mode
1	3900.9	Casing body fracture
2	3076.5	Fracture of the root of external thread
3	3107.2	Fracture of the root of external thread
4	3095.8	Fracture of the root of external thread
5	3090.1	Fracture of the root of external thread

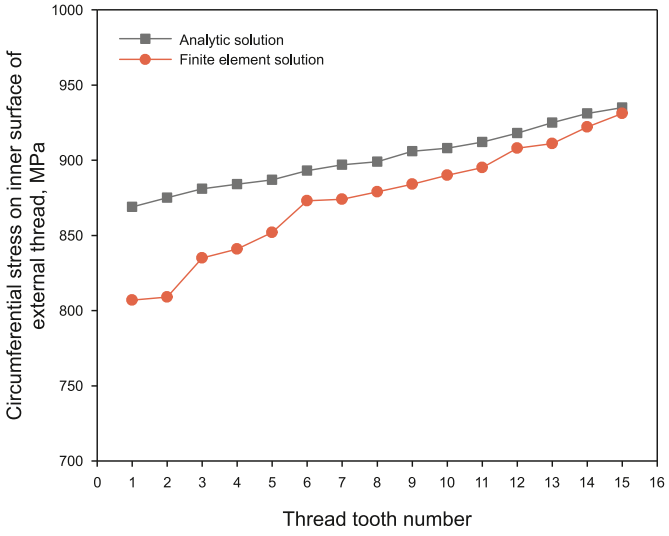

Fig. 16. Comparison of the theoretical and simulation circumferential stresses on the inner surface of joint external thread.

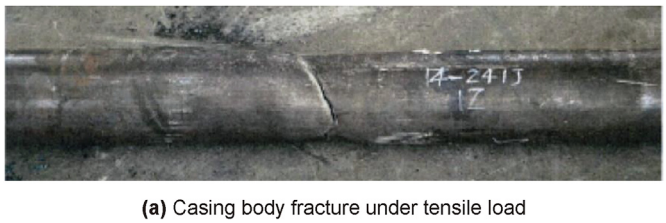

(a) Casing body fracture under tensile load

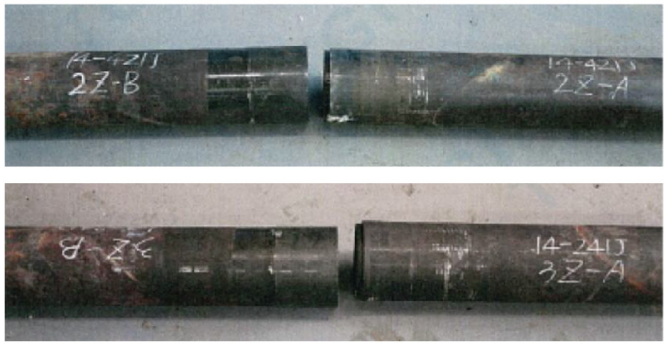

(b) Fracture of the root of external thread under tensile load

Fig. 17. Casing failure mode under tensile load.

Table 5
Results of tensile strength test.

Sample No.	Failure load, MPa	Failure location and failure mode
1	86.2	Casing body collapse
2	89.7	Casing body collapse
3	88.2	Casing body collapse
4	85.8	Casing body collapse
5	87.1	Casing body collapse

Fig. 18. Casing failure mode under external collapse load.

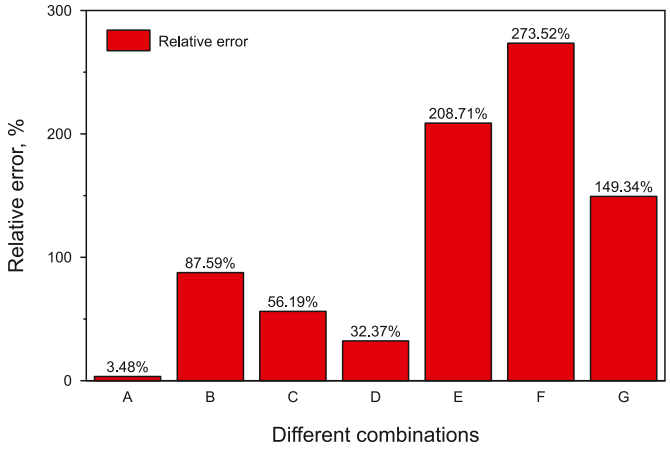

Fig. 19. Relative error of tensile strength with different nonlinearity combinations of the numerical model (A: All three types of nonlinearity; B: Geometric and material nonlinearity; C: Contact and material nonlinearity; D: Contact and geometric nonlinearity; E: Geometric nonlinearity; F: Material nonlinearity; G: Contact nonlinearity).

demonstrates its sophistication.

The above test shows that the CST-ZT extreme line casing meets the actual engineering requirements. At the same time, it has also been successfully applied in different oilfields. Since 2014, Tahe Oilfield has applied CST-ZT extreme line casing for more than ten wells. The casings were successfully placed down the hole and the cementing qualities are good (Wang et al., 2015). In addition, Φ139.7 mm $\times$ 7.72 mm CS-140 CST-ZT extreme line casing has been applied in more than 10 sidetracking horizontal wells in northwest China. The well depth ranged from 5800 to 6500 m. The casing running was smooth and the cementing was successful, meeting the requirements of sidetracking horizontal wells (Huang et al., 2016). The HG-FJ extreme line casing has been used to repair 7 old wells with a maximum depth of 1200 m. All 7 wells' casings were smoothly installed at once, and there was no sticking or slipping during the process (Yang et al., 2017).

According to the simulation results, under the action of axial load, the load borne by each thread tooth is not uniform, and there is stress concentration at the root of each thread tooth, which will affect the strength of the thread connection. Therefore, further optimization of the thread structure can be carried out to improve the stress on the thread tooth. The shape of the thread can be optimized for design to improve the sealing and load-bearing capacity of the connection. For example, increasing the contact area between the tooth peaks and valleys of the thread can improve the sealing effect. Angle and shape of the thread can be adjusted to improve the load-bearing capacity of the connection. Additionally, high-strength and corrosion-resistant metals can be chosen as the thread materials to improve strength and durability. Appropriate heat treatment and surface treatment can also improve the performance of the casing joint.

This work only considers the mechanical reasons for the joint failure. Indeed, various factors can contribute to casing failure, including material properties, local loading conditions, sealing issues, installation and operation problems, and more (Mohammed et al., 2019). Sealing problems in casing are of particular importance as they directly impact the effectiveness of the casing as a barrier (Hao, 2021; Wang et al., 2022). Enhancing the strength of the threaded joint of the casing is a crucial step in improving the sealing performance of the casing (Vishnyakov et al., 2023). In terms of threads, the precision of their profile is an important factor affecting mechanical stress, fatigue safety factor, and contact pressure (Kopei et al., 2021; Onysko et al., 2023). Fatigue of thread joints caused by casing vibration damage can also lead to failure (Mou et al., 2020). The residual strength is also an important aspect. The research on the residual strength of casing joints after wear plays an important role in the analysis of casing sealing and integrity (Liu H. et al., 2022). It should also be mentioned that there are some drawbacks of the extreme line casing. Due to the non-API-standard structure of the extreme line casing, the installation and maintenance process may require more time and human resources. The manufacturing and installation costs of extreme line casings are higher than the conventional casing, which may increase the

Table 6
Compassion of tensile strength.

Tensile strength, kN			Relative error	
Analytical solution	Finite element solution	Test value	Analytical solution vs. test value	Finite element solution vs. test value
2900	3200	3092.4	−6.22%	3.48%

Table 7
Compassion of collapse strength.

Casing body collapsing strength, MPa		Joint collapse strength, MPa		Test value
Analytical solution	Finite element Solution	Analytical solution	Finite element solution	
100	100	108	115	In the test, the casing body is damaged before the joint

overall investment in cementing operations. Also, there is a risk of slipping when using a conventional casing elevator to locate the extreme line casing at the wellhead. Currently, there are special non-coupling casing running devices that can effectively reduce the risk of falling and safely carry out casing operations (Guo et al., 2017).

6. Conclusion

This study addresses the challenges encountered in completing ultra-deep wells through the utilization of the extreme line casing. The focus of the study is on the CST-ZT Φ139.7 mm $\times$ 7.72 mm extreme line casing joint. Finite element analysis, analytical solutions, and experimental tests are combined to investigate the mechanical strengths of the joint. The main conclusions are as follows.

(1) A finite element model is developed to assess the forces and deformations experienced by the extreme line casing joint under axial tension and external collapse load. The analysis incorporates elastic-plastic mechanics to account for geometric and material nonlinearities. The model provides insights into the stress distribution among individual thread teeth when subjected to different tensile forces and external pressures. The finite element simulation results show that under axial tension, the stress distribution on the bearing surface of each thread tooth is uneven, and the equivalent stress at the root of each thread tooth is relatively high. The first and the last thread teeth are the most prone to failure.

(2) By comparing the finite element simulation results with the analytical results, it can be concluded that the tensile strength of the extreme line casing thread tooth decreases linearly with an increase in the number of thread teeth. The circumferential stress at the small end of the external thread is the highest, and failure occurs first at this location.

(3) The tensile strength and collapse strength of the extreme line casing joint are determined using experimental approaches following the API standard. The tensile strength of the joint is 3091.9 kN. The relative error of the tensile strength between the finite element simulation value, analytical value, and indoor test tensile strength value is less than 7%. The tensile strength of the joint reaches 93% of the tensile strength of the casing body, which verifies the accuracy of the finite element model.

(4) The collapse strength of the joints is greater than that of the casing body, indicating that the pipe body fails before the joints. This finding is consistent with the test results, which demonstrate that the pipe body collapses and fails while the joints remain intact. The failure load of the casing body under external collapse load is 87.4 MPa.

(5) The comprehensive analysis conducted in this study contributes to a better understanding of the mechanical behavior and performance of the extreme line casing joint. The findings provide valuable insights for optimizing casing design and improving the reliability and integrity of casing systems in ultra-deep well completions.

CRediT authorship contribution statement

Ji-Yun Zhang: Writing – review & editing, Writing – original draft, Software, Methodology, Investigation, Formal analysis. **Chi Peng:** Writing – review & editing, Writing – original draft, Supervision, Project administration, Methodology, Funding acquisition, Formal analysis, Data curation, Conceptualization. **Jian-Hong Fu:** Writing – original draft, Resources, Project administration, Methodology, Funding acquisition, Conceptualization. **Quan Cao:** Resources, Project administration, Investigation, Data curation. **Yu Su:** Writing – original draft, Data curation, Conceptualization. **Jian-Yun Pang:** Writing – original draft, Supervision, Investigation. **Zi-Qiang Yu:** Resources, Data curation.

Declaration of competing interest

The authors declare that they have no known competing financial interests or personal relationships that could have appeared to influence the work reported in this paper.

Acknowledgments

This work is financially supported by National Natural Science foundation of China (Grant No. 52104006), and Science and Technology Cooperation Project of the CNPC-SWPU Innovation Alliance (Grant No. 2020CX040202). The authors would also like to thank Professor Michael C. Sukop of Florida International University for his suggestions and help.

References

Ahmed, U., Nathan Meehan, D., 2016. Unconventional Oil and Gas Resources: Exploitation and Development. CRC Press.

Bai, H., Dang, T., He, S.L., et al., 2013. Finite element analysis of special thread sealing characteristics under simulated working conditions. Steel Pipe 42 (4), 60–63 (in Chinese).

Bai, H., Lu, B.W., He, S.L., et al., 2015. Finite element analysis of the effect of bearing surface angle on the connection strength of special threaded joints under tensile load. Welded Pipe 38 (9), 26–31. https://doi.org/10.19291/j.cnki.1001-3938.2015.09.007 (in Chinese).

Cao, P., 2013. Calculation analysis and experimental research on the stability of casing and the strength of threaded connections. Master's Thesis. Huazhong University of Science and Technology (in Chinese).

Cao, D.L., Fang, H.L., 2021. Analysis of drilling technology in unconventional oil and gas fields. Petrochem. Technol. 28 (8), 46–47 (in Chinese).

Chen, F., 2014. Analysis of three-dimensional stress characteristics of drill tool joints under complex load conditions. Doctoral Thesis. Shanghai University (in Chinese).

Cirimello, P.G., Otegui, J.L., Carfi, G., et al., 2016. Failure and integrity analysis of casings used for oil well drilling. Eng. Fail. Anal. 75, 1–14. https://doi.org/10.1016/j.engfailanal.2016.11.008.

Cui, Z.Q., 2013. In: Finite element simulation study on expansion sleeve joints. Doctoral Thesis. Xi'an University of Petroleum (in Chinese).

Cui, F., Li, W.J., Gu, Z.L., et al., 2015. Design and study of gas-tight premium threads for tubing and casing. J. Pet. Sci. 133, 208–217. https://doi.org/10.1016/j.petrol.2015.06.007.

Gao, L.X., Wang, H.L., Zhang, Y., et al., 2007. Performance analysis of narrow gap special buckle casing. Nat. Gas. Ind. (11), 58–60+136 (in Chinese).

Guo, Q., 2022. Structural design and analysis of direct connection oil casing joint. Tianjin Metallurgy (1), 46–50 (in Chinese).

Guo, Y.Y., Zhao, Y.A., 2019. Development and application of direct connection oil casing products. Bao Steel Technol. (3), 1–6 (in Chinese).

Guo, X.C., Song, C.H., Xu, X.C., et al., 2017. Non-coupling casing running device. Chinese patent: CN206707629U (in Chinese).

Hao, L., 2021. Analysis on sealing mechanism of casing connection//IOP conference series: earth and environmental science. IOP Publishing 714 (3), 032058. https://doi.org/10.1088/1755-1315/714/3/032058.

Hengel, C.V., 2001. Stress-strain Curve. MIT Press, Cambridge.

Hilbert, L.B., Kalil, I.A., 1992. Evaluation of Premium Threaded Connections Using Finite-Element Analysis and Full-Scale Testing. Louisiana, February, New Orleans. Paper presented at the IADC/SPE Drilling Conference.

Hu, Z.L., 2017. Finite element simulation analysis of casing special threaded joint performance. Steel Tube 46 (5), 64–67 (in Chinese).

Huang, Y., Yang, L.T., Huang, Y., et al., 2016. Research on the development and application of CST-ZT ultra high strength direct connection casing. Steel Pipe 45 (2), 28–32 (in Chinese).

Klementich, E.F., Morey, S.C., Payne, M.L., et al., 1995. Development and acceptance testing of a flush joint casing connection with improved performance properties. SPE Advanced Technology 3 (1), 14–22. https://doi.org/10.2118/26320-PA.

Kopei, V., Onysko, O., Odosii, Z., et al., 2021. Investigation of the Influence of Tapered Thread Profile Accuracy on the Mechanical Stress, Fatigue Safety Factor and Contact pressure//New Technologies, Development and Application IV. Springer International Publishing, Cham, pp. 177–185.

Lambrescu, I., Zisopol, D.G., 2023. Complex analysis of collapse strength for tubulars used in the oil and gas industry. Geoernery Science and Engineering 221, 111275. https://doi.org/10.1016/j.petrol.2022.111275.

Li, H.Z., Lu, X.Q., Hu, L., et al., 2014. Development of 7-5/8 in ultra-high strength direct connection oil casing. Tianjin Metallurgy (2), 5–7 (in Chinese).
Li, Q., Ji, A.M., Liu, W.B., et al., 2018. Finite element analysis on the sealing performance of the casing premium thread connection. Mechanics and Materials Science: Proceedings of the 2016 International Conference on Mechanics and Materials Science (MMS2016), pp. 1172–1178.
Liu, H., Geng, H., Fan, W., et al., 2022. Study on residual strength of casing threaded joint considering wear. International Conference on Mechanisms and Robotics (ICMAR 2022), 12331. SPIE, pp. 1060–1067.
Liu, L.P., Zhang, X.F., Zhang, W.C., et al., 2022. Carbon nanotube enhanced water-based drilling fluid for high temperature and high salinity deep resource development. Petrol. Sci. 19 (2), 916–926. https://doi.org/10.1016/j.petsci.2021.09.045.
Lou, E.R., Liu, H.T., Qin, H., et al., 2021. Study on the factors influencing the external collapse strength of double layer composite casing. Drill. Prod. Technol. 44 (3), 28–32 (in Chinese).
Lu, X., 2017. Analysis of external squeezing load and failure of reservoir casing under complex wellbore conditions. Master's Thesis. Southwest University of Petroleum (in Chinese).
Meza, O.G., Berdasco, J.H., Baptista, N.P., et al., 2016. Technological improvements in OCTG premium casing connections and advancements indesign paradigms to address the challenges present during the exploitation of unconventional hydrocarbon resources: A critical review. Society of Petroleum Engineers Abu Dhabi International Petroleum Exhibition & Conference, Abu Dhabi. UAE 2016-11-07.
Mohammed, A.I., Oyeneyin, B., Atchison, B., et al., 2019. Casing structural integrity and failure modes in a range of well types-a review. J. Nat. Gas Sci. Eng. 68, 102898. https://doi.org/10.1016/j.jngse.2019.05.011.
Mou, Y., Lian, Z., Lin, T., et al., 2020. Study on fatigue of tubing joint thread induced by vibration in HTHP ultradeep wells. J. Pressure Vessel Technol. 142 (3), 031502. https://doi.org/10.1115/1.4046215.
Onysko, O.R., Kusyi, Y.M., Kopei, V.B., et al., 2023. The accuracy of the thread profile depends on the lathe tool angle of inclination. Theoretical investigation//IOP conference series: materials science and engineering. IOP Publishing 1277 (1), 012018.
Pan, X.Y., 2019. Research on Integrity of Casing Special Threaded Joints. Master's Thesis. Southwest Petroleum University (in Chinese).
Shahani, A.R., Sharifi, S.M.H., 2009. Contact stress analysis and calculation of stress concentration factors at the tool joint of a drill pipe. Mater. Des. 30 (9), 3615–3621. https://doi.org/10.1016/j.matdes.2009.02.022.
Shi, J.Q., Gao, L.X., Zhao, K.F., et al., 1998. Discussion on the performance, evaluation and application of coupling less casing. Petroleum Drilling and Production Technology 20 (5), 30–37 (in Chinese).
Silva, T.B., Junior, E.T.L., Gouveia, L.P., 2019. Structural reliability applied to analytical modeling of the tensile strength of standard api casing connections. Brazilian Journal of Petroleum and Gas 13 (4), 301–307. https://doi.org/10.5419/bjpg2019-0025.
Sun, X., Pei, J.J., Xie, B., et al., 2016. Study on the resistance to external compression of thin oil well casing under non-uniform load. Petroleum Pipe and Instrument 2 (5), 69–72. https://doi.org/10.19459/j.cnki.61-1500/te.2016.05.019 (in Chinese).
Sun, J.A., Zhang, Z.D., Cao, Q., 2022. Development and application of 88.9 mm (3(1/2)″) BG-FJU small casing direct-connection joints. Petroleum Industry Technical Supervision 38 (5), 63–67 (in Chinese).
Vishnyakov, P., Yangirov, F., Ibragimov, D., et al., 2023. Ways to increase the sealness of screwed joints of casing string. AIP Conference Proceedings. AIP Publishing LLC, 2700 (1), 020018.
Wang, C., Sun, R., Wang, Y.J., 2015. Application research of expansion tailpipe hanger and direct coupling casing in Tahe Oilfield. Inner Mongolia Petrochemical (20), 35–37 (in Chinese).
Wang, H.T., Huang, J.B., Gao, L., et al., 2014. Development of direct connection special tubing thread. Xinjiang Petroleum and Natural Gas 10 (4), 90–92 (in Chinese).
Wang, J., Liu, H.Q., Qian, G.B., et al., 2021. Mechanisms and capacity of high-pressure soaking after hydraulic fracturing in tight/shale oil reservoirs. Petrol. Sci. 18, 546–564. https://doi.org/10.1007/s12182-020-00524-z.
Wang, X.C., Shao, M., 1997. Fundamental Principles and Numerical Methods of Finite Element Method, Second Edition. Tsinghua University Press (in Chinese).
Wang, C., Liu, X., Wang, H., et al., 2022. Research on sealing performance of special thread of tubing under complex load. In: Journal of Physics: Conference Series, 2230. IOP Publishing, 2230 (1), 012034.
Xiang, T., 2016. Design and Evaluation of a New 374.65 Mm BC Casing Joint in Air Drilling. Master's Thesis. China University of Petroleum (Beijing (in Chinese).
Xu, H.L., 2015. Research on Strength and Sealing Theory of Oil Casing Special Thread Connection. Doctoral Thesis. Southwest Petroleum University (in Chinese).
Xu, Z.Q., Wang, B.B., Yan, Y.F., 2019. Integrity evaluation analysis of casing premium connection. Press. Vessel Technol. 36 (5), 35–42+13.
Xu, H., Yang, B., Zhang, Z., et al., 2019. Special considerations to calculate joint strength of premium connections. J. Petrol. Sci. Eng. 182, 106295. https://doi.org/10.1016/j.petrol.2019.106295.
Yang, F.R., Chen, C.Q., Xue, Z.J., et al., 2017. Development and application of HG-FJ economical direct connection sleeve products. Steel Pipe 46 (6), 73–76. https://doi.org/10.19938/j.steelpipe.1001-2311.2017.06.023 (in Chinese).
Zeng, P., 2004. Finite Element Analysis and Application. Tsinghua University Press (in Chinese).
Zhang, H.W., 2004. Finite Element Analysis and CAE Technology Basis. Tsinghua University Press (in Chinese).
Zhang, L., 2020. Talking about the development and utilization of unconventional oil and gas resources at home and abroad. Chemical Management (14), 4–5 (in Chinese).
Zhang, W., Chen, H., 2019. Technology status and prospect of unconventional oil and gas development. Petrochem. Technol. 26 (12), 223+227 (in Chinese).
Zhang, Y., Lian, Z.H., Zhou, M., et al., 2019. Numerical simulation research on sealing performance of special thread of oil casing. Pressure Vessel 36 (12), 23–29 (in Chinese).
Zhuang, Z., 2009. Finite Element Analysis and Application Based on ABAQUS. Tsinghua University Press (in Chinese).